



Title	Antioxidative copper sinter bonding under thermal aging utilizing reduction of cuprous oxide nanoparticles by polyethylene glycol
Author(s)	Matsuda, Tomoki; Yamada, Seigo; Okubo, Shio et al.
Citation	Journal of Materials Science. 2023, 58(40), p. 15617-15633
Version Type	VoR
URL	<a href="https://hdl.handle.net/11094/93223">https://hdl.handle.net/11094/93223</a>
rights	This article is licensed under a Creative Commons Attribution 4.0 International License.
Note	

*The University of Osaka Institutional Knowledge Archive : OUKA*

<https://ir.library.osaka-u.ac.jp/>

The University of Osaka



# Antioxidative copper sinter bonding under thermal aging utilizing reduction of cuprous oxide nanoparticles by polyethylene glycol

Tomoki Matsuda<sup>1,\*</sup> , Seigo Yamada<sup>1</sup>, Shio Okubo<sup>1</sup>, and Akio Hirose<sup>1</sup>

<sup>1</sup> Division of Materials and Manufacturing Science, Graduate School of Engineering, Osaka University, 2-1 Yamadaoka, Suita 565-0871, Japan

**Received:** 7 June 2023

**Accepted:** 20 September 2023

**Published online:**  
19 October 2023

© The Author(s), 2023

## ABSTRACT

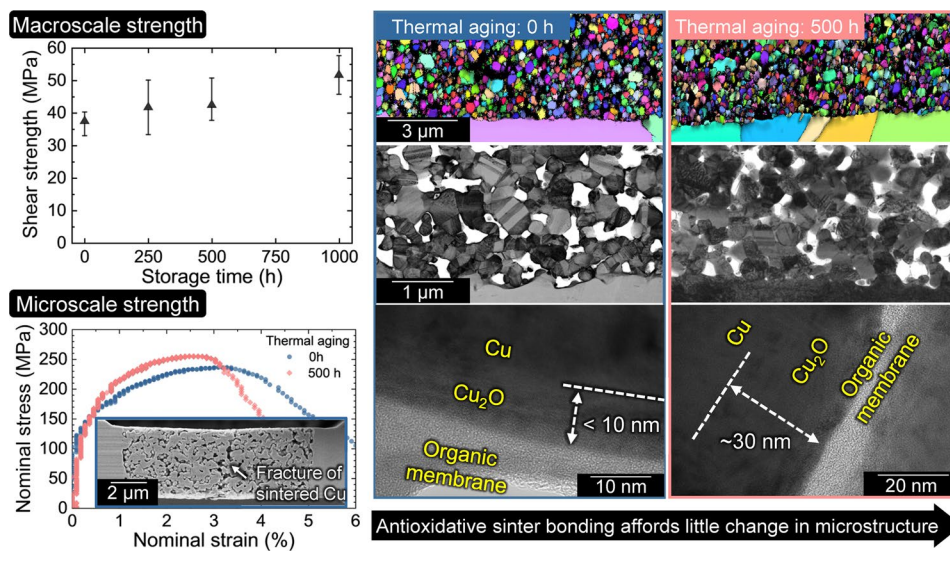
Durability of sintered Cu joints under thermal aging in the air was investigated for the reduction of Cu<sub>2</sub>O using Cu<sub>2</sub>O/polyethylene glycol (PEG) mixture. Thermal analysis of the Cu<sub>2</sub>O/PEG paste showed that the molecular weight of PEG influences the redox reaction and the subsequent bonding related to the combustion of the reducing organic solvent. Sintered Cu joints using PEG 400 exhibited high joint strength (above 30 MPa) in shear tests, even for the bonding temperature of 280 °C. The sintered Cu joints exhibited slightly increased strength during thermal aging at 250 °C in air, which was also confirmed by the microscale tensile test used for evaluating the fracture behavior of the sintered Cu structure. Microstructural analysis, including the evaluation of the crystal orientation, revealed a small change in the microstructure of sintered joints during aging. Transmission electron microscopy revealed the presence of organic membranes on slightly oxidized sintered Cu grains before thermal aging, and additional oxidation was observed after thermal aging. The progress of sintering during thermal aging in vacuum was different than that in air. It was considered that the formation of a thin Cu<sub>2</sub>O layer, controlled by the presence of organic membranes, contributed to the suppression of Cu sintering.

Handling Editor: N. Ravishankar.

Address correspondence to E-mail: t-matsu@mapse.eng.osaka-u.ac.jp

<https://doi.org/10.1007/s10853-023-08976-5>

## GRAPHICAL ABSTRACT



## Introduction

Sinter bonding using metal particles has attracted growing attention as a promising technology for manufacturing power modules using semiconductors that operate at temperatures above 150 °C [1]. As sinter materials, Ag and Cu are widely used in various morphologies, such as sizes ranging from nanoscale to microscale [2–4], shapes (e.g., particles and flakes) [4–6], and composites (e.g., mixture and core–shell structures) [7, 8]. Cu sinter bonding has been recently studied to obtain sintered joints with high thermal and migration resistivities compared to Ag sinter bonding [9–11]. In particular, changes in the mechanical, electrical, and thermal properties of sintered joints during thermal aging are important, as the power modules are subjected to such high-temperature environments.

There are many reports on changes in the microstructure and properties of sintered Cu joints during thermal aging [9, 12, 13]. It is noteworthy that the oxidation of sintered Cu during thermal aging generally occurs in a high-temperature environment. Gao et al. [14] reported that the strength of sintered Cu joints was improved by the progress of Cu sintering during the thermal aging, whereas the joints exhibited increased resistivity and insulation with the formation of Cu oxides. Furthermore, the thermal conductivity of the Cu oxides was lower than that of

Cu. Although the mechanical properties of joints are maintained, the oxidation of Cu thus degrades the thermal and electrical properties which are required in power modules, forcing the sintering process under an inert gas or reducing gas atmospheres [9, 10, 15–17]. Therefore, it is important to form sintered joints with oxidation resistance for sintering in air.

Organic substances or carbon can provide significant resistance against the oxidation of metals [18–20]. Cu nanowires, which require oxidation resistance to lower electrical resistance, are generally used with organic substances to prevent thermal oxidation [21–23]. This can also be explained by the catalytic activity of Cu in the oxidation of organic substances [24]. Furthermore, some researchers have utilized acid treatment on Cu particles for the sintering process. Liu et al. [25] reported that the formic acid treatment of Cu nanoparticles resulted in a highly sintered body by eliminating surface oxidation. Gao et al. [26] reported that ascorbic acid treatment of Cu particles provides them with self-reduction and self-protection characteristics during sintering. Thus, organic substances play a significant role in achieving robust sintered Cu joints by preventing the oxidation of Cu during thermal aging.

In this study, we evaluate the robustness of sintered Cu joints bonded using Cu<sub>2</sub>O nanoparticles and polyethylene glycol (PEG) during thermal aging under ambient air. The reduction of oxide particles

by reducing agents generates metal nanoparticles, which can be utilized for the sinter bonding process (hereafter referred to as reduction sinter bonding) because of their high sinterability [27–32]. Several studies on sinter bonding using the reduction of Cu oxide [31–33], including the in-situ formation of oxides [16], have been reported. Some organic solvents, such as alcohols, can act as reducing agents in oxidation–reduction (redox) reactions, that is, the polyol process. After the redox reaction, the organic solvents can remain as either unreacting solvent or product of redox reaction. As for the reduction of  $\text{Cu}_x\text{O}$  (with particle size in nanometers), it has been reported that Cu can be produced after the reduction of CuO to  $\text{Cu}_2\text{O}$  [31, 34].  $\text{Cu}_2\text{O}$  particles are more suitable than CuO particles for reduction sinter bonding to avoid aggregation of produced particles. Therefore, the reduction sinter bonding using  $\text{Cu}_2\text{O}$  and PEG may suppress the oxidation of sintered Cu joints owing to the existence of organic matters after the bonding process.

## Experimental procedure

Commercial  $\text{Cu}_2\text{O}$  nanoparticles (Furukawa Chemicals Co., Ltd.) were used as sintering materials. Figure 1 shows the field-emission scanning electron microscopy (FE-SEM) image of  $\text{Cu}_2\text{O}$  nanoparticles. PEGs ( $\text{C}_{2n}\text{H}_{4n+2}\text{O}_{n+1}$ ) with different average molecular weights of 200, 400, and 1000 were used as reducing organic solvents. To evaluate the behavior of pastes during heating, simultaneous thermogravimetry and differential thermal analysis measurements (TG–DTA) (Rigaku, TG8120) were performed at a heating rate of  $60\text{ }^\circ\text{C}/\text{min}$  in air and  $\text{N}_2$  atmospheres. For the TG–DTA

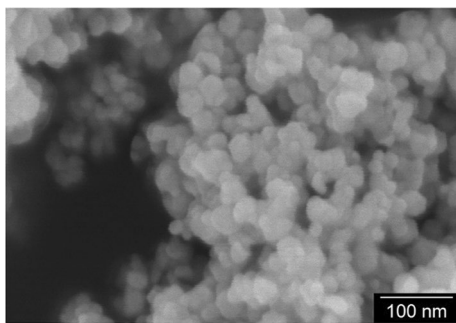


**Figure 1** FE-SEM image of  $\text{Cu}_2\text{O}$  nanoparticles.

measurements, a sufficient amount of PEG was mixed with  $\text{Cu}_2\text{O}$  to investigate its behavior.

Figure 2 shows the schematic illustrations of bonding specimen and evaluation of strength. For the bonding experiments, bare Cu disks of sizes  $5\text{ mm } \varphi \times 2\text{ mm t}$  and  $10\text{ mm } \varphi \times 2\text{ mm t}$  were used as the upper and lower bonding substrates as shown in Fig. 2a. The  $\text{Cu}_2\text{O}$  paste for bonding was prepared by mixing  $\text{Cu}_2\text{O}$  particles,  $330\text{ }\mu\text{L/g}$  PEG 400, and  $280\text{ }\mu\text{L/g}$  terpineol as a viscosity modifier. The  $\text{Cu}_2\text{O}$  paste was applied to the surface of the lower Cu substrate with a thickness of  $50\text{ }\mu\text{m}$ , and the upper substrate was placed on the paste. The samples were heated to the bonding temperature of  $260\text{--}300\text{ }^\circ\text{C}$  at a rate of  $1\text{ }^\circ\text{C}/\text{s}$  in an infrared heating furnace under an air atmosphere and held for 30 min at a pressure of 5 MPa. The samples were cooled using forced air. Thermal aging was performed through a thermal storage test at  $250\text{ }^\circ\text{C}$  in ambient air for 0–1000 h and in a vacuum for 0–500 h.

The strength of the Cu joints was measured using a shear test with a displacement rate of  $0.5\text{ mm/s}$  as shown in Fig. 2b. The joint microstructure was observed using FE-SEM (Hitachi, S-4800). The crystal orientation of the microstructure was analyzed using

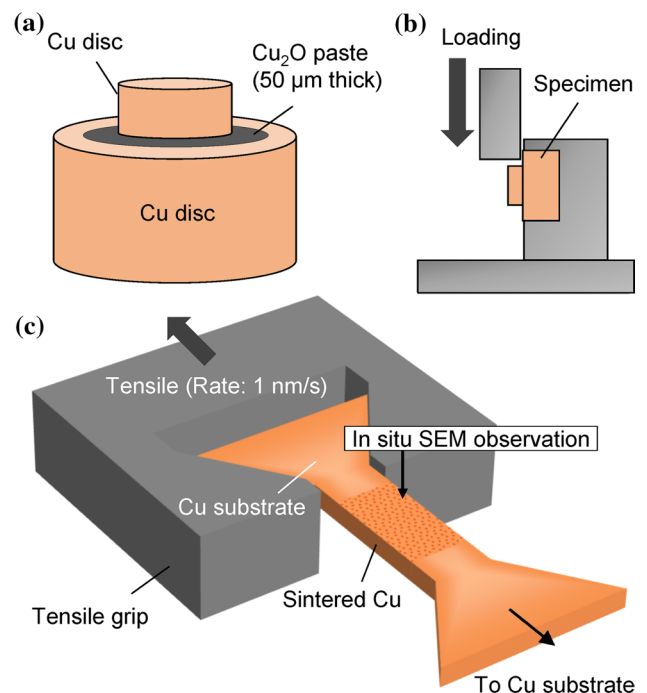
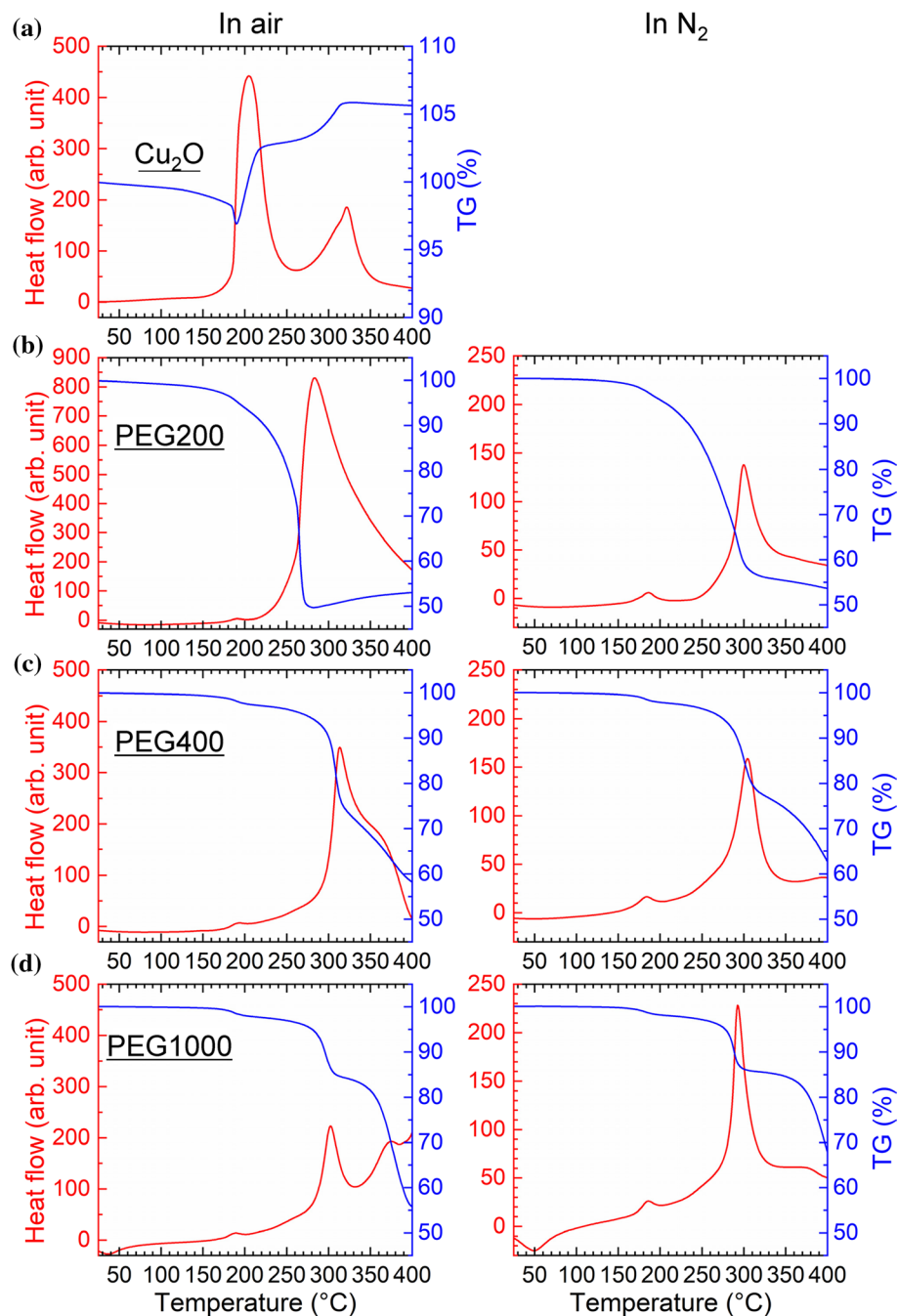


**Figure 2** Schematic illustrations of bonding specimen and mechanical test. **a** Bonding specimen. **b** Shear test. **c** Microscale tensile test for the evaluation of sintered layer.

**Figure 3** TG–DTA results of **a** the  $\text{Cu}_2\text{O}$  nanoparticles and the  $\text{Cu}_2\text{O}$  paste prepared using, **b** PEG 200, **c** PEG 400, and **d** PEG 1000 performed in the air and  $\text{N}_2$  atmospheres.



electron backscatter diffraction (EBSD) (EDAX). The joint cross-section was prepared by Ar ion milling (Hitachi, IM4000, and JEOL, SM-09010). The detailed microstructure of the cross-section of the joint was observed using transmission electron microscopy (TEM) (Thermo Fisher Scientific, Talos F200i). The TEM specimens were prepared using focused ion beam scanning electron microscopy (FIB-SEM, Thermo Fisher Scientific, Scios 2 DualBeam).

The strength of the sintered layer before and after thermal aging was measured using an in-situ uniaxial microscale tensile test [35, 36]. Dog-bone-shaped specimens were fabricated using FIB-SEM, and microscale tensile tests were performed on the specimens using a nanoindenter (FemtoTools, FT-NMT04) under FE-SEM observation as shown in Fig. 2c. The tensile tests were performed in displacement-controlled mode at a displacement rate of 1 nm/s.

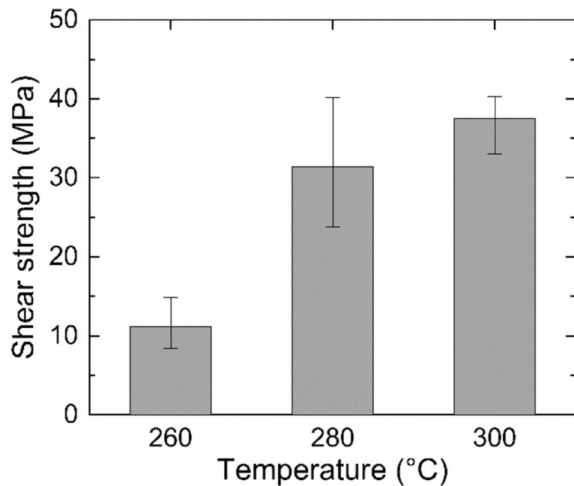


**Figure 4** Shear strength of the Cu joints bonded at 260–300 °C.

## Results and discussion

### Cu<sub>2</sub>O reduction sinter bonding

Figure 3 shows the results of the TG–DTA analysis of the Cu<sub>2</sub>O nanoparticles and the Cu<sub>2</sub>O/PEG mixed paste. The TG–DTA results for the Cu<sub>2</sub>O particles in air exhibited a large exothermic peak at approximately 190 °C with a weight loss of approximately 3%. The exothermic peak is considered to correspond to a combustion reaction of the organic film adhering to the surface of the Cu<sub>2</sub>O nanoparticles. After the weight loss, a weight increase of approximately 6% was observed in the temperature range before and after the exothermic peak. Thereafter, an exothermic peak with a weight increase of approximately 3% was observed at 310 °C, and the weight remained almost constant in the temperature range above 310 °C.

Assuming that Cu<sub>2</sub>O was oxidized to CuO during the temperature rise, the mass increased by approximately 11.2% according to the chemical reaction  $2\text{Cu}_2\text{O} + \text{O}_2 \rightarrow 4\text{CuO}$ . In the TG–DTA results for the Cu<sub>2</sub>O particles, assuming that the paste after organic film removal at 190 °C was comprised of Cu<sub>2</sub>O, the particles showed a weight increase of approximately 9.3% during the temperature increase. The weight increase could be justified by considering that the particles after organic film removal were partially CuO.

In other words, the two exothermic reactions accompanying the weight gain observed during the temperature increase of the Cu<sub>2</sub>O powder can be attributed to the heat of oxidation of Cu<sub>2</sub>O. In particular, the

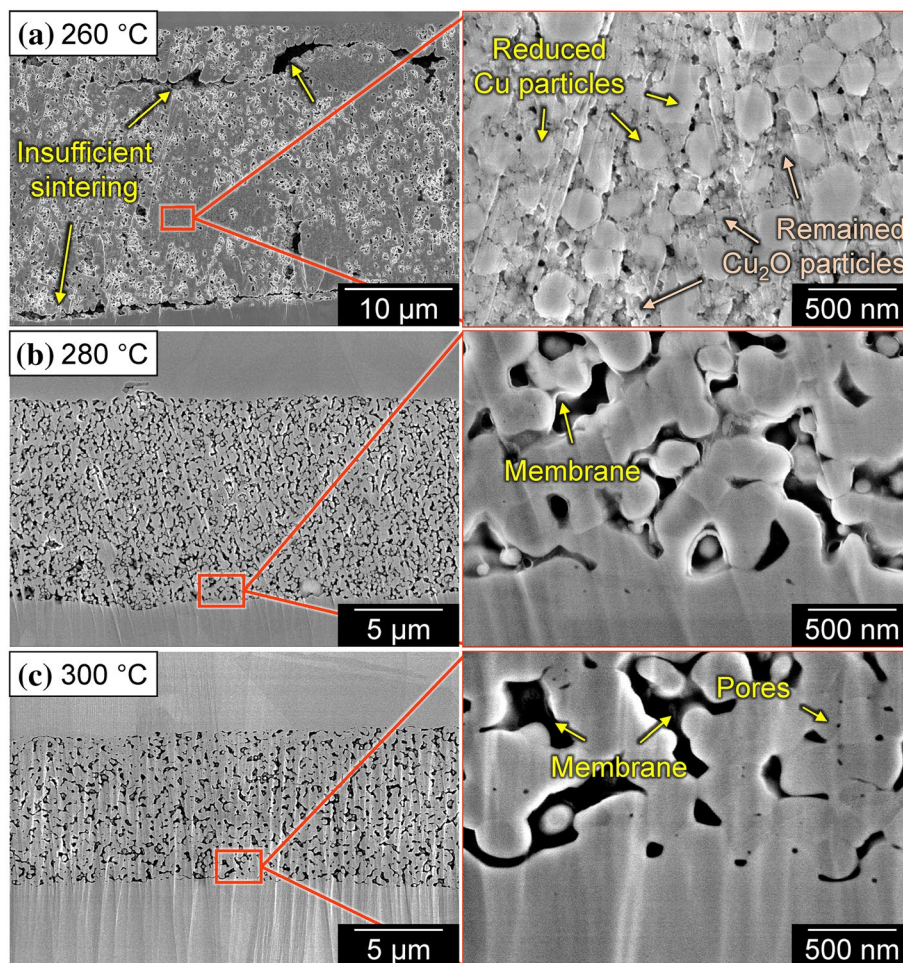
reaction at approximately 200 °C is considered to be due to the oxidation of Cu<sub>2</sub>O by the heat of combustion of organic matter, while the reaction at approximately 310 °C is considered to be due to the oxidation of Cu<sub>2</sub>O powder during the temperature increase.

Figure 3b–d show the results of TG–DTA measurements performed in N<sub>2</sub> and air atmospheres on the Cu<sub>2</sub>O pastes prepared using PEG solvents with different numbers of main chains. The TG–DTA results in the N<sub>2</sub> atmosphere indicated that the redox reaction between the Cu<sub>2</sub>O particles and PEG was accompanied by an exothermic reaction. Moreover, the redox reaction between the Cu<sub>2</sub>O particles and the organic solvent occurred in the N<sub>2</sub> atmosphere. The TG–DTA results in the air indicated that the reaction is different from that in the N<sub>2</sub> atmosphere, depending on the solvent species. In the case of PEG 200, which has a short main chain, an exothermic reaction with a steep weight loss was observed at lower temperatures than in N<sub>2</sub>, and a further increase in the reaction temperature increased the weight increase. These results suggest that PEG 200 burned at 280 °C in the paste, and Cu or Cu<sub>2</sub>O was oxidized by the air atmosphere. In contrast, PEG 400 and PEG 1000, which have longer main chains, showed a reduction reaction similar to that in a N<sub>2</sub> atmosphere, and combustion of the organic solvent after the reduction reaction was also observed. The two pastes showed different combustion behaviors of the residual solvent; that is, in the case of PEG 400, the combustion reaction occurred with a reduction reaction, whereas in the case of PEG 1000, the combustion reaction occurred above 350 °C. Residual organic solvents inhibit particle-to-particle and particle-to-substrate sintering. Therefore, the use of PEG 400 is considered effective in reducing the reduction behavior and residual solvent in Cu<sub>2</sub>O reduction sintering bonding.

The relationship between the temperature and shear strength of the joints prepared using the PEG 400 paste is shown in Fig. 4. The joint strength was lower than 15 MPa at 260 °C, whereas the average joint strength was higher than 30 MPa at temperatures above 280 °C.

Figure 5 shows the cross-section of the joints at different bonding temperatures. For the joint prepared at 260 °C (Fig. 5a), many voids were observed in the sintered layer, particularly at the lower Cu substrate/sintered layer interface, where defects were observed. The magnified image of the sintered layer reveals that the layer was constructed of both an aggregate of reduced Cu particles, which had grown

**Figure 5** Cross-sectional FE-SEM images of Cu joints bonded at 260–300 °C before thermal aging.



to approximately 200 nm, and fine  $\text{Cu}_2\text{O}$  particles of several tens of nanometers in the unsintered state covering the surrounding area. For the joint prepared at 280 °C (Fig. 5b), interfacial bonding with the substrate was achieved, and sintering between submicron particles progressed, accompanied by the disappearance of nanoparticles. For the joint prepared at 300 °C (Fig. 5c), the particles were further sintered, and the substrate and sintered layer were integrated at the interface.

Figure 6 shows the results of X-ray diffraction (XRD) measurements performed on the fracture surfaces of the joints after the shear tests at various temperatures. The fracture surfaces mainly contained  $\text{Cu}_2\text{O}$  and Cu particles at 260 °C, whereas at 280 °C and above, the diffraction peaks of  $\text{Cu}_2\text{O}$  disappeared, and only those of CuO were present. The XRD profile of the  $\text{Cu}_2\text{O}$  nanoparticles shows only a peak of  $\text{Cu}_2\text{O}$ . These results indicate that  $\text{Cu}_2\text{O}$  remains in the sintered layer at the bonding temperature of 260 °C for a holding time of 5 min because

of the insufficient reduction reaction between  $\text{Cu}_2\text{O}$  particles and PEG 400, despite the reduction of  $\text{Cu}_2\text{O}$  to Cu.

The TG–DTA results in Fig. 3 show that the starting temperature of the reduction reaction was 260 °C, indicating that the reduction and combustion reactions occurred insufficiently at 260 °C. In this case,  $\text{Cu}_2\text{O}$  and the solvent tended to remain and form defects because they hindered the sintering of the reduced Cu particles during the bonding process. In contrast, the joint strength can be improved by Cu particle sintering through sufficient reduction and combustion reactions during the bonding process at temperatures above 260 °C.

### Characterization of sintered Cu joints after thermal aging

Figure 7 shows the results of thermal aging of different Cu joints at 250 °C in the air; the Cu joints used

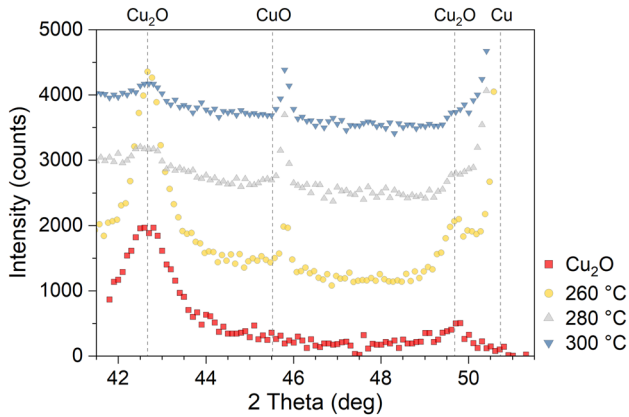


**Figure 6** XRD patterns obtained from the fractured surface of Cu joints bonded at 260–300 °C. The XRD pattern of Cu<sub>2</sub>O particles is also shown as a reference.

in this analysis were bonded at 280 and 300 °C. As shown in Fig. 7a, both joints exhibited a slight increase in strength with aging time, whereas the strength of the joint bonded at 300 °C was higher than that of the joint bonded at 280 °C. Typical fracture surfaces of Cu joints bonded at 300 °C before and after thermal aging are shown in Fig. 7b–d. Each fracture surface shows the ductility of the sintered Cu. In contrast to the joints before aging, the joints after aging exhibited progressive sintering of Cu.

Figure 8 shows the cross-sections of the Cu joints bonded at 300 °C after thermal aging. Compared to the

joints before thermal aging, as shown in Fig. 5, the Cu joints after thermal aging exhibited a slight change in the microstructure; that is, the sintering of Cu grains progressed slightly, while the porosity of the sintered layer was almost the same. These images show no boundary between the sintered Cu layer and the Cu substrate, revealing that the oxidation of Cu did not occur during the test. The Cu joints contained dark-colored membranes on the surface of the Cu grains before aging, as shown in Fig. 5c.

Figure 9 shows the EBSD results in the form of inverse pole figure (IPF) and pole figure (PF) maps of the Cu the joints bonded at 300 °C before and after aging at 250 °C. Table 1 lists the average grain sizes and twinning ratios estimated from the EBSD results. The morphology of the sintered layer slightly changed during aging, even though the dense region is composed of fine grains. The pole figure maps reveal no anisotropy in the texture of the sintered layer.

A slight microstructural change in the sintered Cu layer was observed during thermal aging in the air. A microscale tensile test was performed on the sintered Cu layer to evaluate the change in the mechanical properties before and after aging at 250 °C for 500 h, and Fig. 10a shows the nominal stress–nominal strain curves of these joints. After aging, the strength and elongation of the Cu joints slightly increased and decreased, respectively, compared to those before aging. Figure 10b, c show the representative in-situ FE-SEM observation results of

**Figure 7** Thermal aging at 250 °C in the air of sintered Cu joints bonded at 280 and 300 °C using the Cu<sub>2</sub>O/PEG 400 paste. **a** Shear strength and fracture surface of the joints bonded at 300 °C after aging for **b** 0 h, **c** 250 h, and **d** 1000 h.

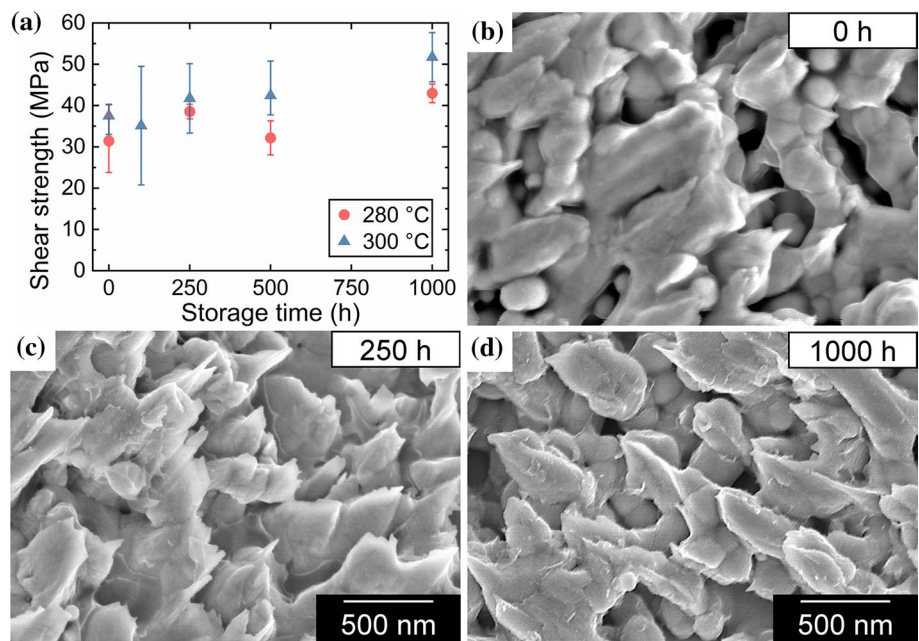
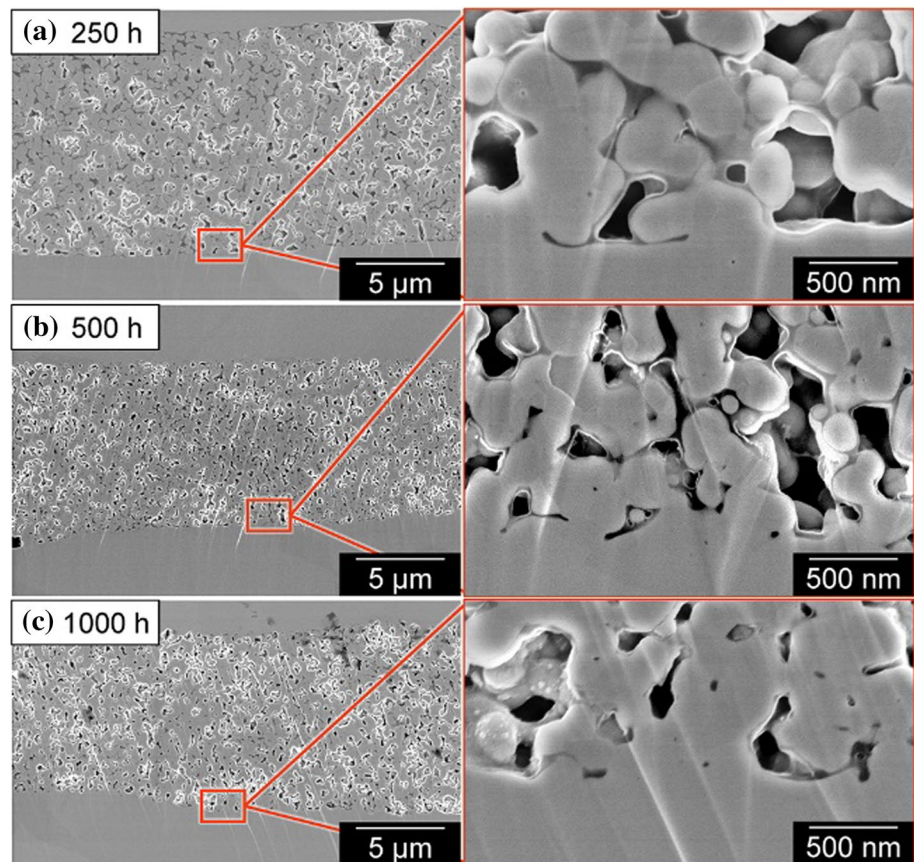


**Figure 8** Cross-sectional FE-SEM images of the Cu joints bonded at 300 °C after thermal aging in the air at 250 °C for **a** 250 h, **b** 500 h, and **c** 1000 h.



the fracture behavior in the sintered Cu layer before and after aging, respectively. The fracture behavior in both layers was evaluated during the microscale tensile test, before the tensile test, just after the maximum nominal stress, and during decreasing nominal stress. The porosities of the sintered layer thermally aged for 0 and 500 h before the tensile test were 21.6% (Fig. 10b) and 21.2% (Fig. 10c), respectively. Although these sintered layers were only elongated without fracture up to the maximum stress, fracture of the sintered layer started to occur through a decrease in stress. After that, the nominal stress decreased by the reduction of area owing to the progress of fracture. This was also confirmed through the images after the tensile test showing a narrow fracture region of a few micrometers for both joints. The fracture position differs depending on the joint; that is, the fracture position is at the center of the joint before aging and the root of the joint after aging, which would be due to the difference in the shape of the dog-bone specimen. The cross-sections of both joints after the tensile test revealed that fractures occurred inside the grains with ductility and at the sinter interfaces with little ductility. These results indicate that the

sintered interfaces or Cu grains fracture because the sintered Cu grains deform with elongation. The sintered Cu interface was found to be stiff, regardless of thermal aging. Such a stiff interface with little ductility was also observed in the sintered Ag structure, although it exhibited ductility after thermal aging because of the sintering progress [37]. Thus, the microscale tensile test revealed no significant change in the mechanical properties of the sintered Cu layer before and after aging, which is consistent with the slight change in the microstructure.

### Investigation of factors responsible for microstructural changes in sintered Cu joints

The above results demonstrate that the mechanical properties of the sintered Cu slightly increased with thermal aging in air, whereas there was little change in the microstructure of the sintered layer, as confirmed by FE-SEM observations. It has been reported that thermal aging enhances the mechanical properties of sintered Cu [14], where the sintered Cu layer is oxidized through thermal aging in an air atmosphere. The

**Figure 9** IPF and PF maps of Cu joints thermally aged in the air at 250 °C for **a** 0 h, **b** 250 h, and **c** 500 h.

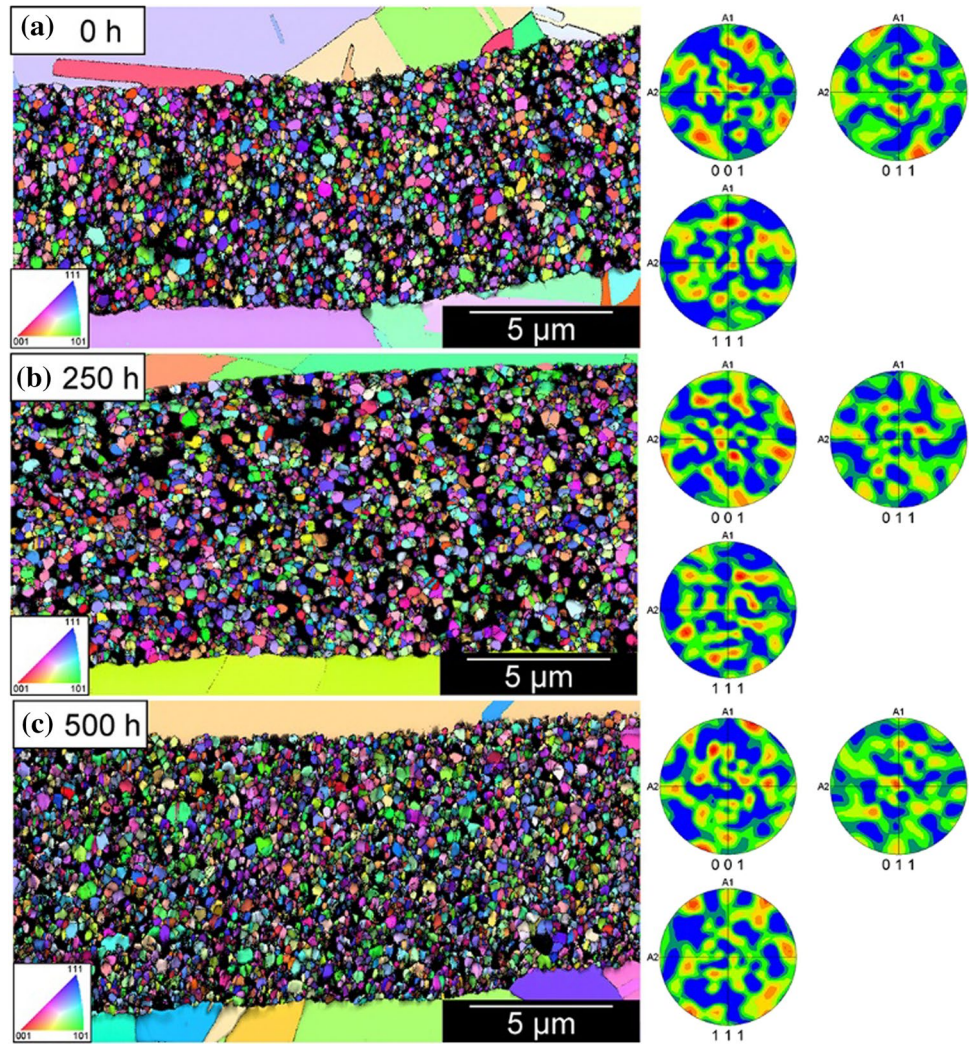


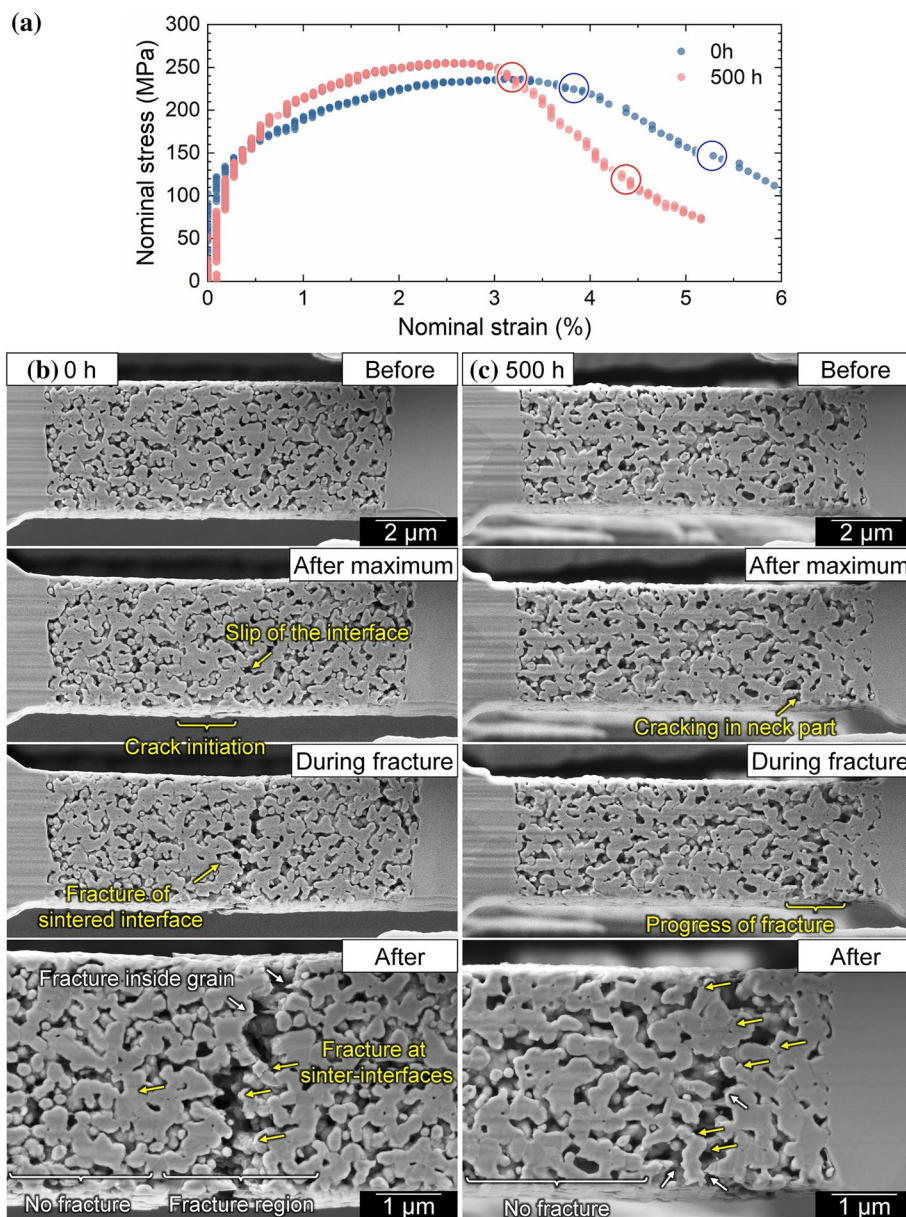
**Table 1** Grain sizes and twinning ratios of Cu joints after thermal aging in air

Aging time (h)	0	250	500
Grain size (nm)	310	350	300
Twinning ratio (%)	41.4	47.7	41.9

oxidation of Cu below 300 °C generally occurs with the formation of Cu<sub>2</sub>O [38]. Oxidation induces densification of the sintered layer and an increase in the joints owing to its volume change following the Pilling–Bedworth ratio, although it also involves an increase in resistivity. Thus, Cu<sub>2</sub>O reduction sinter bonding can suppress the oxidation of sintered Cu. To elucidate the conditions of oxidation and suppression factor, TEM observations were performed on the joints before and after thermal aging in the air.

Figure 11 shows the cross-sectional TEM images of the joints before thermal aging. Consistent with the FE-SEM results, a porous structure was formed by sintering of the reduced Cu particles. At the joint interface between the sintered Cu layer and the Cu substrate shown in Fig. 11b, the sintered Cu grains were bonded to the substrate without an obvious oxide layer. Moreover, the interface exhibited a disordered area, such as a grain boundary. Therefore, it was found that the interfacial bonding between the reduced Cu and the Cu substrate was established without the oxidation of the substrate owing to the reducing organic solvent at the bonding temperature of 300 °C. Figure 11c shows the representative sintered Cu microstructure. Membrane areas, corresponding to that confirmed by FE-SEM observations, were present around the sintered grains. Figure 11d shows the magnified view of the edge of sintered Cu grains. The amorphous

**Figure 10** Results of microscale tensile testing of Cu joints before and after thermal aging at 250 °C in air. **a** Stress–strain curves of both the Cu joints. FE-SEM images during a tensile test of the Cu joints **b** before aging and **c** after aging for 500 h.

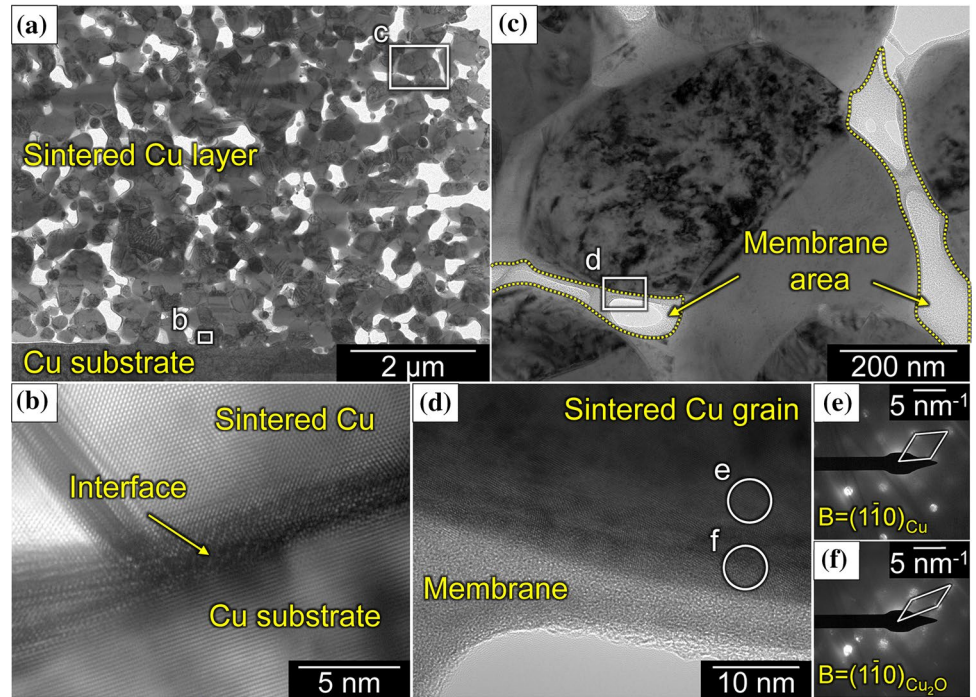


membrane covered the Cu grains, and different crystal structures were observed at the surface of the Cu grains. Figure 11e, f show the electron diffraction patterns obtained from regions e and f shown in Fig. 11d, representing the formation of a  $\text{Cu}_2\text{O}$  layer with thickness below 10 nm on the surface of Cu grains. While the film regions shown in Fig. 11 were composed of a single phase, some regions were composed of a composite phase. Figure 12 shows the results of the EDS analysis of the membrane composed of a composite phase. The membrane was composed of carbon-containing Cu nanoparticles. This result indicates that the membrane corresponds to the organic residue formed

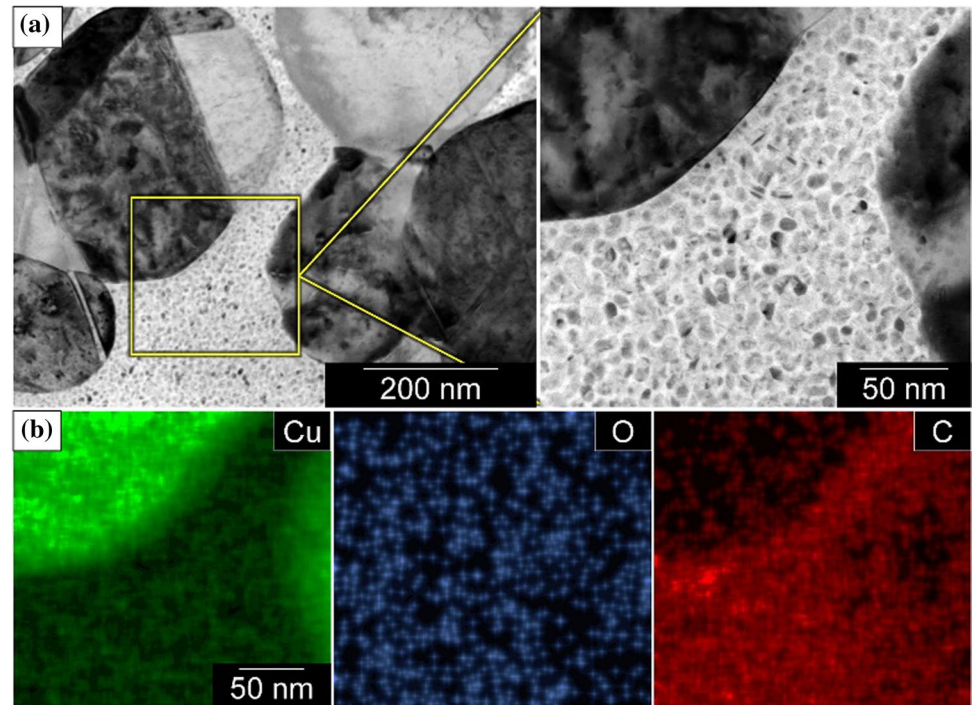
during the bonding process after the redox reaction, and the reduced unsintered Cu nanoparticles were confined within the organic residue.

Figure 13 shows the cross-section of the joints after thermal aging at 250 °C for 500 h in air. No significant aging-induced changes in the microstructure of the sintered layer were observed (Fig. 13a). The interface between the sintered Cu layer and the Cu substrate did not exhibit the formation of an interfacial layer, as shown in Fig. 13b, revealing that the substrate did not oxidize during aging. Figure 13c, d show the microstructure of the sintered Cu layer. The membrane area observed before aging remained

**Figure 11** TEM images of the cross-section of the Cu sintered joint before thermal aging: **a** overview, **b** interface between the Cu substrate and the sintered Cu layer, **c** representative image of the sintered Cu layer, **d** the edge of a sintered Cu grain showing the presence of membrane on the surface. **e**, **f** Electron diffraction patterns of the surface of the sintered Cu layer.



**Figure 12** EDS results of the membrane formed around the sintered Cu grains.

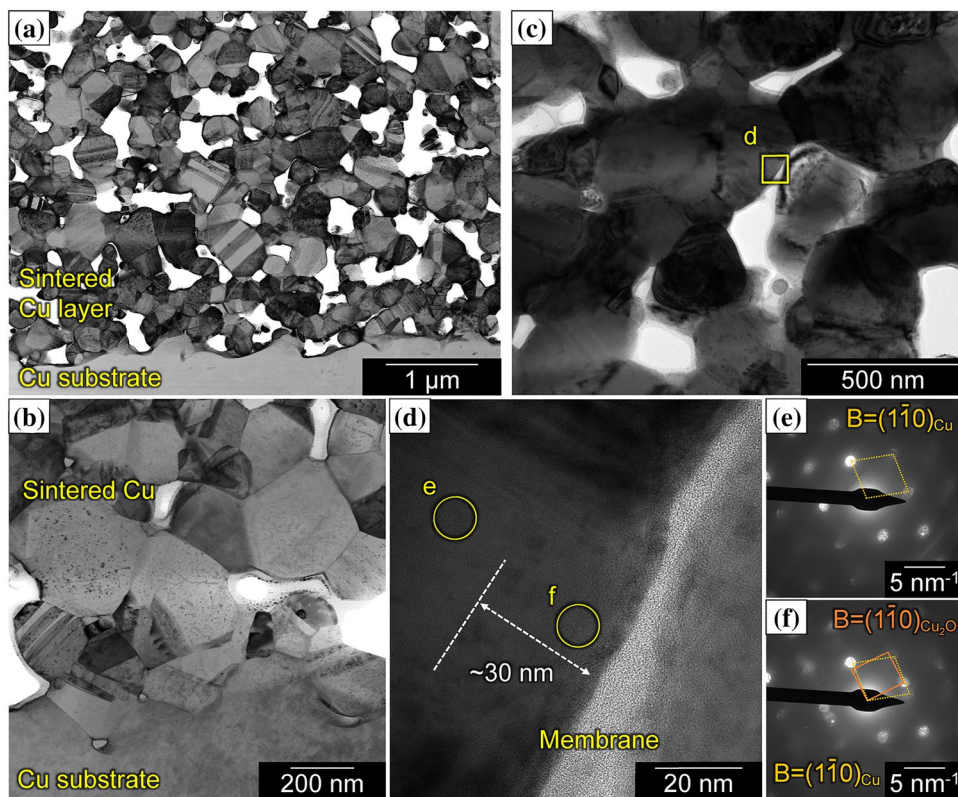


intact after aging. The electron diffraction patterns of regions e and f (Fig. 13e, f) and fast Fourier-transform patterns revealed that a  $\text{Cu}_2\text{O}$  layer was formed within 30 nm from the surface of the sintered Cu grains. Therefore, sinter bonding through

the reduction of  $\text{Cu}_2\text{O}$  using PEG 400 suppresses the oxidation of the sintered Cu layer.

The oxidation of Cu in the air is generally dependent on temperature. Choudhary et al. [38] reported that Cu oxidizes to  $\text{Cu}_2\text{O}$  below 300 °C and to CuO

**Figure 13** TEM and STEM images of the cross-section of Cu sintered joint after thermal aging at 250 °C for 500 h in the air: **a** overview, **b** interface between the Cu substrate and the sintered Cu layer, **c** representative image of the sintered Cu layer, **d** magnified view of the edge of the sintered Cu. **e** and **f** Electron diffraction patterns of the surface of the sintered Cu layer.



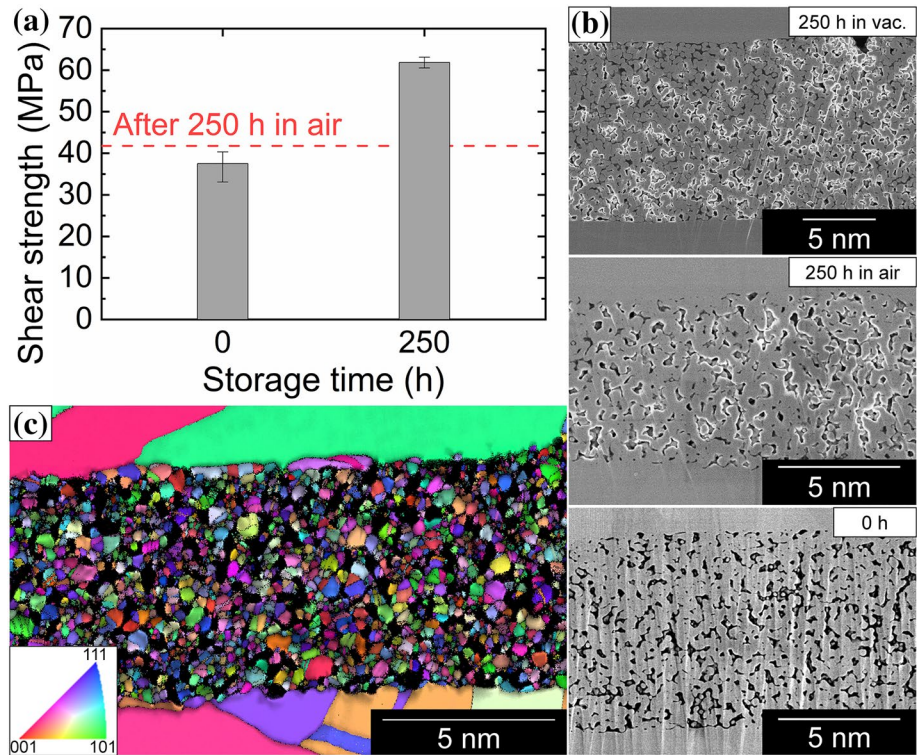
above 330 °C. Hence, the formation and growth behaviors of the  $\text{Cu}_2\text{O}$  layer on the sintered Cu grains owing to the thermal aging at 250 °C in the present study are considered to follow the general oxidation process of Cu. The small change in the sintered Cu structure during the thermal aging could be due to its delayed oxidation by the residue of the redox reaction and suppression of the sintering process. One of the products of polyalcohol in the polyol process is a carboxylic acid, which covers the surface of sintered grains or shows combustion. Covered organic matter sometimes suppresses the oxidation of metals [39–41]. Wang reported that lactic acid treatment of Cu nanoparticles could prevent the oxidation of Cu by forming Cu salts [39]. Thus, it is hypothesized that the presence of both oxide and organic matter on the surface of the sintered grains enables robust sinter joints during thermal aging under an air atmosphere. The sintering behavior under a non-oxidizing atmosphere was evaluated to validate the effect of these factors on sintering suppression.

Figure 14 shows the results of the characterization of the sintered Cu joints after aging at 250 °C under vacuum. The joint strength increased to 60 MPa after

aging in a vacuum, and it was higher than that in the air. Cross-sectional FE-SEM and IPF images of joints in a vacuum, shown in Fig. 14b, c, show that the porosity of the joints decreased from 16.2 to 11.7%, and the grain size of the joints (340 nm) was almost the same as that of the joints aged in the air (350 nm). These results reveal that the densification of the sintered Cu layer preferentially occurred during thermal aging in a vacuum instead of grain growth, indicating that sintering during aging in a vacuum, which does not involve oxidation, should be attributed to the surface free energy of the sintered Cu grains or particles.

The sintering of particles is generally categorized as (a) grain growth involving the reduction of particle surfaces and (b) densification attributed to the change of particle surfaces to grain boundaries during necking. When the grain boundary energy is lower than the surface energy, the grain growth is not so preferential that particles become closer with increasing grain boundaries. Chen et al. [5] reported the grain growth of a sintered Ag layer during a thermal storage test at 250 °C. Kim et al. [42] reported an increase in twin density of Ag grains per length with grain growth for a sintered Ag layer during a thermal cycling test. In contrast, thermal aging in a vacuum did not result

**Figure 14** Characterization of joints after thermal aging in vacuum for 250 h: **a** shear strength test results of the joints before and after aging. **b** Comparison between joint cross-sections after aging for 250 h in a vacuum, 250 h in the air (corresponding to Fig. 8a), and 0 h (corresponding to Fig. 5c). **c** IPF map of the Cu joints after aging for 500 h in a vacuum.



in grain growth but densification in the sintered Cu layer. Furthermore, there was a slight increase in the twinning ratio, which also revealed no tendency for grain growth. The results of Cu sintering in a vacuum for Cu<sub>2</sub>O reduction bonding are different from the sintering behavior confirmed in the case of Ag; that is, Cu sintering proceeds with the formation of grain boundaries driven by the surface energy.

The suppression of sintering observed for thermal aging in the air could be due to factors unrelated to the sintering of the particles, as mentioned above. Focusing on the microstructural changes during thermal aging in air and under vacuum, the difference in the sintering behavior between them is caused by the formation of a Cu<sub>2</sub>O layer on the surface of the Cu particles. The wettability of Cu generally increases with the oxidation as reported by many studies [43, 44]. These reports reveal that the oxidation of the Cu surface during the thermal aging reduces the surface energy of Cu. It is known that lowering ratio of surface energy to grain boundary energy leads to the tendency to grain growth rather than densification in sintering [45–47]. This knowledge supports the robust sintered Cu joints during thermal aging in the air. On the other hand, the densification would progress in vacuum owing

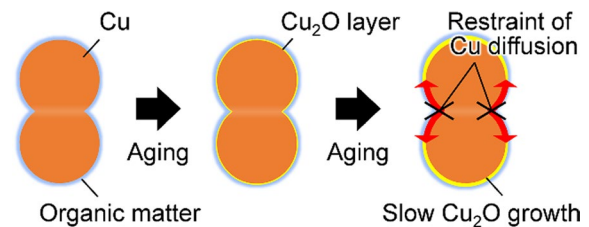


**Figure 15** Schematic illustration of the oxidation process in Cu<sub>2</sub>O sinter joints.

to a little oxidation, which corresponded to the prior studies [12, 14].

Figure 15 illustrates the formation process of the sintered Cu structure in reduction sinter bonding using Cu<sub>2</sub>O/PEG during thermal aging in air. Cu<sub>2</sub>O reduction sinter bonding forms a sintered Cu structure through necking among the grown Cu particles with sizes of several hundreds of nanometers after the formation of reduced Cu particles. The surfaces of the sintered Cu grains were slightly oxidized and covered by the organic product of the redox reaction. The oxidation of Cu grains was suppressed by the organic product, leading to slight growth of the Cu<sub>2</sub>O layer on the sintered Cu grains, which consequently decreased the driving force for the densification of Cu

grains. Hence, the microstructural changes attributed to both the volume change during oxidation and the progress of sintering became smaller, and long-time heat resistance was obtained in the Cu<sub>2</sub>O reduction sinter bonding process. Consequently, the control of the surface morphology of sintered grains using oxidation and organic matter should be effective in forming anti-oxidative and robust Cu-sintered structures against thermal aging. Such structures play an important role in obtaining good thermal, electrical, and mechanical properties for power modules.

## Conclusions

We analyzed the robustness of sintered Cu joints under thermal aging in the air using Cu<sub>2</sub>O reduction sinter bonding. The main findings are summarized as follows:

- (1) Cu<sub>2</sub>O reduction sinter bonding for high joint strength requires a reducing organic solvent that remains after the redox reaction is completed and that the excess organic residue of the redox reaction does not remain during bonding.
- (2) Thermal aging of sintered Cu joints in air exhibited a slight change in their mechanical properties, including the macroscale shear strength and microscale tensile strength. The microstructure was evaluated by EBSD, and local fracture behavior was evaluated by microscale tensile tests. A small progress of sintering and a slight change in the microstructure were observed for the sintered Cu joints.
- (3) The formation of organic matter on the surface of Cu in the Cu<sub>2</sub>O reduction sinter bonding process, using a mixture of Cu<sub>2</sub>O and PEG, suppresses Cu oxidation.
- (4) The slight oxidation of the sintered Cu surface enhances the robustness of the sintered Cu structure owing to the small progress of sintering attributed to the lowering of surface energy.

## Acknowledgements

This work was supported in part by Japan Society for the Promotion of Science (JSPS) KAKENHI [Grant Number 22H01832].

## Author contributions

TM: conceptualization, data curation, formal analysis, funding acquisition, investigation, methodology, writing—original draft. SY: data curation, formal analysis, investigation, writing—original draft. SO: investigation. AH: supervision, writing—review and editing.

## Funding

Open access funding provided by Osaka University.

## Data and code availability

The datasets generated and analyzed during the current study are available from the corresponding author upon reasonable request.

## Declarations

**Conflict of interest** The authors declare that they have no known competing financial interests or personal relationships that could have appeared to influence the work reported in this paper.

**Open Access** This article is licensed under a Creative Commons Attribution 4.0 International License, which permits use, sharing, adaptation, distribution and reproduction in any medium or format, as long as you give appropriate credit to the original author(s) and the source, provide a link to the Creative Commons licence, and indicate if changes were made. The images or other third party material in this article are included in the article's Creative Commons licence, unless indicated otherwise in a credit line to the material. If material is not included in the article's Creative Commons licence and your intended use is not permitted by statutory regulation or exceeds the permitted use, you will need to obtain permission directly from the copyright holder. To view a copy of this licence, visit <http://creativecommons.org/licenses/by/4.0/>.

## References

- [1] Chalker PR (1999) Wide bandgap semiconductor materials for high temperature electronics. *Thin Solid Films* 343–344:616–622. [https://doi.org/10.1016/S0040-6090\(98\)01672-1](https://doi.org/10.1016/S0040-6090(98)01672-1)
- [2] Ide E, Angata S, Hirose A, Kobayashi KF (2005) Metal–metal bonding process using Ag metallo-organic nanoparticles. *Acta Mater* 53:2385–2393. <https://doi.org/10.1016/j.actamat.2005.01.047>
- [3] Bai JG, Lu G-Q (2006) Thermomechanical reliability of low-temperature sintered silver die attached SiC power device assembly. *IEEE Trans Device Mater Reliab* 6:436–441. <https://doi.org/10.1109/TDMR.2006.882196>
- [4] Li J, Li X, Wang L et al (2018) A novel multiscale silver paste for die bonding on bare copper by low-temperature pressure-free sintering in air. *Mater Des* 140:64–72. <https://doi.org/10.1016/j.matdes.2017.11.054>
- [5] Chen C, Suganuma K, Iwashige T et al (2018) High-temperature reliability of sintered microporous Ag on electroplated Ag, Au, and sputtered Ag metallization substrates. *J Mater Sci Mater Electron* 29:1785–1797. <https://doi.org/10.1007/s10854-017-8087-8>
- [6] Roh MH, Nishikawa H, Tsutsumi S et al (2017) Effect of temperature and substrate on shear strength of the joints formed by sintering of micro-sized Ag particle paste without pressure. *J Mater Sci Mater Electron* 28:7292–7301. <https://doi.org/10.1007/s10854-017-6414-8>
- [7] Hsiao CH, Kung WT, Song JM et al (2017) Development of Cu–Ag pastes for high temperature sustainable bonding. *Mater Sci Eng A* 684:500–509. <https://doi.org/10.1016/j.msea.2016.12.084>
- [8] Jia Q, Zou G, Wang W et al (2020) Sintering mechanism of a supersaturated Ag–Cu nanoalloy film for power electronic packaging. *ACS Appl Mater Interfaces* 12:16743–16752. <https://doi.org/10.1021/acsami.9b20731>
- [9] Chen TF, Siow KS (2021) Comparing the mechanical and thermal-electrical properties of sintered copper (Cu) and sintered silver (Ag) joints. *J Alloys Compd* 866:158783. <https://doi.org/10.1016/j.jallcom.2021.158783>
- [10] Gao Y, Takata S, Chen C et al (2019) Reliability analysis of sintered Cu joints for SiC power devices under thermal shock condition. *Microelectron Reliab* 100–101:113456. <https://doi.org/10.1016/j.microrel.2019.113456>
- [11] Lee CJ, Kang DG, Hwang BU et al (2021) Fabrication of an IPL-sintered Cu circuit and its electrochemical migration behavior. *J Alloys Compd* 863:158726. <https://doi.org/10.1016/j.jallcom.2021.158726>
- [12] Xie J, Shen J, Deng J, Chen X (2020) Influence of aging atmosphere on the thermal stability of low-temperature rapidly sintered Cu nanoparticle paste joint. *J Electron Mater* 49:2669–2676. <https://doi.org/10.1007/s11664-020-07951-z>
- [13] Koga S, Nishikawa H, Saito M, Mizuno J (2020) Fabrication of nanoporous Cu sheet and application to bonding for high-temperature applications. *J Electron Mater* 49:2151–2158. <https://doi.org/10.1007/s11664-019-07916-x>
- [14] Gao Y, Jiu J, Chen C et al (2022) Oxidation-enhanced bonding strength of Cu sinter joints during thermal storage test. *J Mater Sci Technol* 115:251–255. <https://doi.org/10.1016/j.jmst.2021.10.047>
- [15] Lin SK, Nagao S, Yokoi E et al (2016) Nano-volcanic eruption of silver. *Sci Rep* 6:34769. <https://doi.org/10.1038/srep34769>
- [16] Gao R, He S, Li J et al (2020) Interfacial transformation of preoxidized Cu microparticles in a formic-acid atmosphere for pressureless Cu–Cu bonding. *J Mater Sci Mater Electron* 31:14635–14644. <https://doi.org/10.1007/s10854-020-04026-x>
- [17] Huang HJ, Wu X, Zhou MB, Zhang XP (2021) Superior strength and strengthening mechanism of die attachment joints by using bimodal-sized Cu nanoparticle paste capable of low-temperature pressureless sintering. *J Mater Sci Mater Electron* 32:3391–3401. <https://doi.org/10.1007/s10854-020-05086-9>
- [18] Datta KKR, Kulkarni C, Eswaramoorthy M (2010) Aminoclay: a permselective matrix to stabilize copper nanoparticles. *Chem Commun* 46:616–618. <https://doi.org/10.1039/b919421e>
- [19] Jin M, Zhang H, Wang J et al (2012) Copper can still be epitaxially deposited on palladium nanocrystals to generate core–shell nanocubes despite their large lattice mismatch. *ACS Nano* 6:2566–2573. <https://doi.org/10.1021/nn2050278>
- [20] Shi L, Wang R, Zhai H et al (2015) A long-term oxidation barrier for copper nanowires: graphene says yes. *Phys Chem Chem Phys* 17:4231–4236. <https://doi.org/10.1039/c4cp05187d>
- [21] Chu CR, Lee C, Koo J, Lee HM (2016) Fabrication of sintering-free flexible copper nanowire/polymer composite transparent electrodes with enhanced chemical and mechanical stability. *Nano Res* 9:2162–2173. <https://doi.org/10.1007/s12274-016-1105-y>
- [22] Lian L, Dong D, Wang H, He G (2019) Highly reliable copper nanowire electrode with enhanced transmittance and robustness for organic light emitting diodes. *Org Electron* 65:70–76. <https://doi.org/10.1016/j.orgel.2018.11.002>
- [23] Zhang T, Daneshvar F, Wang S, Sue HJ (2019) Synthesis of oxidation-resistant electrochemical-active copper nanowires using phenylenediamine isomers. *Mater Des*

- 162:154–161. <https://doi.org/10.1016/j.matdes.2018.11.043>
- [24] Taher A, Kim DW, Lee IM (2017) Highly efficient metal organic framework (MOF)-based copper catalysts for the base-free aerobic oxidation of various alcohols. *RSC Adv* 7:17806–17812. <https://doi.org/10.1039/c6ra28743c>
- [25] Liu J, Chen H, Ji H, Li M (2016) Highly conductive Cu–Cu joint formation by low-temperature sintering of formic acid-treated Cu nanoparticles. *ACS Appl Mater Interfaces* 8:33289–33298. <https://doi.org/10.1021/acsami.6b10280>
- [26] Gao Y, Li W, Chen C et al (2018) Novel copper particle paste with self-reduction and self-protection characteristics for die attachment of power semiconductor under a nitrogen atmosphere. *Mater Des* 160:1265–1272. <https://doi.org/10.1016/j.matdes.2018.11.003>
- [27] Hirose A, Tatsumi H, Takeda N et al (2009) A novel metal-to-metal bonding process through in-situ formation of Ag nanoparticles using Ag<sub>2</sub>O microparticles. *J Phys Conf Ser* 165:012074. <https://doi.org/10.1088/1742-6596/165/1/012074>
- [28] Asama K, Matsuda T, Ogura T et al (2017) Materials science and engineering a low-temperature metal-to-alumina direct bonding process utilizing redox reaction between silver oxide and organic agent. *Mater Sci Eng A* 702:398–405. <https://doi.org/10.1016/j.msea.2017.07.034>
- [29] Motoyama K, Matsuda T, Sano T, Hirose A (2018) AlN-to-metal direct bonding process utilizing sintering of Ag nanoparticles derived from the reduction of Ag<sub>2</sub>O. *J Electron Mater* 47:5780–5787. <https://doi.org/10.1007/s11664-018-6504-2>
- [30] Matsuda T, Inami K, Motoyama K et al (2018) Silver oxide decomposition mediated direct bonding of silicon-based materials. *Sci Rep* 8:10472. <https://doi.org/10.1038/s41598-018-28788-x>
- [31] Yao T, Matsuda T, Sano T et al (2018) In situ study of reduction process of CuO paste and its effect on bondability of Cu-to-Cu joints. *J Electron Mater* 47:2193–2197. <https://doi.org/10.1007/s11664-017-6049-9>
- [32] Yonezawa T, Tsukamoto H, Matsubara M (2015) Low-temperature nanoredox two-step sintering of gelatin nanoskin-stabilized submicrometer-sized copper fine particles for preparing highly conductive layers. *RSC Adv* 5:61290–61297. <https://doi.org/10.1039/c5ra06599b>
- [33] Yamagiwa D, Matsuda T, Furusawa H et al (2021) Pressureless sinter joining of bare Cu substrates under forming gas atmosphere by surface-oxidized submicron Cu particles. *J Mater Sci Mater Electron* 32:19031–19041. <https://doi.org/10.1007/s10854-021-06418-z>
- [34] Unutulmazsoy Y, Cancellieri C, Lin L, Jeurgens LPH (2022) Reduction of thermally grown single-phase CuO and Cu<sub>2</sub>O thin films by in-situ time-resolved XRD. *Appl Surf Sci* 588:152896. <https://doi.org/10.1016/j.apsusc.2022.152896>
- [35] Matsuda T, Yamada S, Takeuchi A et al (2021) Fracture behavior of thermally aged Ag–Cu composite sinter joint through microscale tensile test coupled with nano X-ray computed tomography. *Mater Des* 206:109818. <https://doi.org/10.1016/j.matdes.2021.109818>
- [36] Matsuda T, Seo R, Hirose A (2023) Highly strong interface in Ag/Si sintered joints obtained through Ag<sub>2</sub>O–Ag composite paste. *Mater Sci Eng A* 865:144647. <https://doi.org/10.1016/j.msea.2023.144647>
- [37] Watanabe T, Takesue M, Matsuda T et al (2020) Thermal stability and characteristic properties of pressureless sintered Ag layers formed with Ag nanoparticles for power device applications. *J Mater Sci Mater Electron* 31:17173–17182. <https://doi.org/10.1007/s10854-020-04265-y>
- [38] Choudhary S, Sarma JVN, Pande S et al (2018) Oxidation mechanism of thin Cu films: a gateway towards the formation of single oxide phase. *AIP Adv*. <https://doi.org/10.1063/1.5028407>
- [39] Wang X, Zhang Z, Feng Y, Xiao F (2022) Anti-oxidative copper nanoparticle paste for Cu–Cu bonding at low temperature in air. *J Mater Sci Mater Electron* 33:817–827. <https://doi.org/10.1007/s10854-021-07352-w>
- [40] Mou Y, Liu J, Cheng H et al (2019) Facile preparation of self-reducible Cu nanoparticle paste for low temperature Cu–Cu bonding. *JOM* 71:3076–3083. <https://doi.org/10.1007/s11837-019-03517-5>
- [41] Zuo Y, Shen J, Hu Y, Gao R (2018) Improvement of oxidation resistance and bonding strength of Cu nanoparticles solder joints of Cu–Cu bonding by phosphating the nanoparticle. *J Mater Process Technol* 253:27–33. <https://doi.org/10.1016/j.jmatprotec.2017.11.001>
- [42] Kim D, Lee S, Chen C et al (2021) Fracture mechanism of microporous Ag-sintered joint in a GaN power device with Ti/Ag and Ni/Ti/Ag metallization layer at different thermo-mechanical stresses. *J Mater Sci* 56:9852–9870. <https://doi.org/10.1007/s10853-021-05924-z>
- [43] Hong KT, Imadojemu H, Webb RL (1994) Effects of oxidation and surface roughness on contact angle. *Exp Therm Fluid Sci* 8:279–285. [https://doi.org/10.1016/0894-1777\(94\)90058-2](https://doi.org/10.1016/0894-1777(94)90058-2)
- [44] Nam Y, Ju YS (2013) A comparative study of the morphology and wetting characteristics of micro/nanostructured Cu surfaces for phase change heat transfer applications. *J Adhes Sci Technol* 27:2163–2176. <https://doi.org/10.1080/01694243.2012.697783>
- [45] Shi JL (1999) Thermodynamics and densification kinetics in solid-state sintering of ceramics. *J Mater Res* 14:1398–1408. <https://doi.org/10.1557/JMR.1999.0190>
- [46] Abdeljawad F, Bolintineanu DS, Cook A et al (2019) Sintering processes in direct ink write additive manufacturing: a

mesoscopic modeling approach. *Acta Mater* 169:60–75. <https://doi.org/10.1016/j.actamat.2019.01.011>

- [47] Hussein O, Alghalayini M, Dillon SJ, Abdeljawad F (2021) Unraveling the role of grain boundary anisotropy in sintering: implications for nanoscale manufacturing. *ACS Appl Nano Mater* 4:8039–8049. <https://doi.org/10.1021/acsanm.1c01322>

**Publisher's Note** Springer Nature remains neutral with regard to jurisdictional claims in published maps and institutional affiliations.